Jurnal Teknologi

Full paper

Numerical Investigation for Resistance Characteristics of LNG Carrier

A. Y. Sian, A. Maimun*, A. Priyanto, Yasser M. Ahmed, M. Nakisa, Rahimuddin

Marine Technology Centre, Universiti Teknologi Malaysia, 81310 UTM Johor Bahru, Johor, Malaysia

*Corresponding author: adi@fkm.utm.my

Article history

Received :10 March 2013
Received in revised form :
30 March 2014
Accepted :3 May 2014

Graphical abstract

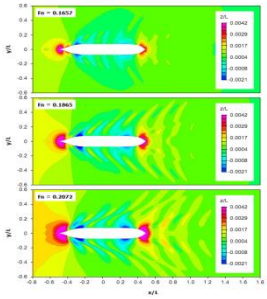

Abstract

Reynolds Averaged Navier-Stokes (RANS) computations are conducted with general purpose CFD solver Fluent to examine the resistance and viscous free surface flow of Liquefied Natural Gas (LNG) carrier hull form in calm water. Shear-stress transport k-ω turbulence model and multiphase volume of fluid (VOF) free surface employed. The resistance characteristics and wave profile of the LNG model also investigated. Model tests were conducted in towing tank for validation of the computed results. Overall results agree fairly well with experimental data, reveals the feasibility of RANS method in practical prediction of LNG resistance characteristics.

Keywords: Resistance; computer fluid dynamics (CFD); RANS; free surface

1.0 INTRODUCTION

Investigation on the hydrodynamic performance of marine vehicles is a great important topic in marine engineering, due to its important in practical design process. Model testing remains the most effective method in investigation of ship hydrodynamics during the past decades. Nowadays, rapid development in computer technology has made numerically prediction of ship hydrodynamic performance possible. Even though model tests are still inevitable in case of validation purposes, prediction of hydrodynamic forces can be achieved via computational fluid dynamics (CFD) calculations.

Reynolds Averaged Navier-Stokes (RANS) method coupled with turbulence model has been widely used in the past. A number of numerical studies relating to resistance issues have been carried out based on RANS equations with early example found in Larsson[1,2] and Bertram[3]. Since then, numerical error and resolution of flow details have been significantly improved. Taking advantage of modern computer, CFD software is now available commercially with the solution turnaround time dramatically reduced.

Feasibility of CFD has been demonstrated at Gothenburg 2010 Workshop on CFD in Ship Hydrodynamics with reports of resistance predictions within a few percents on average from experimental results for three different hull form: DTMB 5415, KVLCC2 and KCS[4], reveals that CFD techniques have matured sufficiently in modelling of viscous ship hydrodynamics, at least ship resistance can be obtained with reasonable confidence. Survey performed by ITTC[5] also recognises the CFD elements of importance among ship hydrodynamics community with the prediction of resistance as the most dominant application among the respondents.

In the case of resistance prediction, accurate prediction of free surface around ship hull is crucial and often views as a precursor for accuracy in wave resistance prediction. Conventional method often assumes free surface in the simulation as flat and rigid to avoid the complication presented by the sea/air interface. However, in absence of wave surface, total resistance computedwould only consist of frictional resistance and viscous pressure resistance, with wave making resistance neglected[6,7].

Numerous researches have been conducted recently on the free-surface flow around the ship. Two major approaches in modelling of free surface are the level-set function and Volume of Fluid (VOF). In the former method, a signed distance from the interface is defined in the domain and the free surface location is given by an isosurface from level set function. This method was previously used to examine the resistance as described in Hino *et al.*[8] and Kim *et al.*[9]. The prediction can be done in single phase level set approach as in Wilson *et al.*[10] or multiphase approach where both water and air is solved, for instance in work of Stern *et al.*[11]. Only water is computed in single phase level set approach and thus it is robust and used for a variety of ship flows problems. A more recent application of single-phase level set approach is

that of Maki *et al.*[12] where free surface around a surface effect ship tracked with RANS.

In Volume of Fluid (VOF), transport equation is solved in additional to the conservation equations of mass and momentum in each cell for volume fraction of one fluid. A value of unity in cells volume fraction represents complete filled of water in cell, and value zero for complete filled of air. Free surface would be represented with an isosurface plotted at cells with volume fraction 0.5 in this sense.

Accuracy of this method has been demonstrated in Zwart *et al.*[13] in steady and transient diffraction calculation of wave profile and drag for flow around Wigley and DTMB 5415 hulls with good experimental data agreement. Additional example of VOF can be found in Fonfach *et al.*[14] for optimization of series 60 container vessel using RANS based code. An interesting aspect of this paper is where the free surface is addressed with prismatic layer mesh in addition to unstructured tetrahedral grid used with the grid sensitivity studied.

To effectively utilizing outcome from CFD with confidence, it would be essential to perform validation with experimental results. In this study, the resistance and viscous free surface flow of LNG carrier hull form in calm water are examined. Resistance simulations were conducted in using general purpose RANS solver Fluent V14. Model tests were conducted in towing tank to validate the numerical results in resistance. This paper is organized as follows. First, the mathematicalmodel is presented. This is followed by descriptions of the numerical and experimental methods. The computational results are shown in the results section for analysis, and discussions. Finally, concludingremarks are made in the conclusion section.

■2.0 NUMERICAL METHODS

The flow around ship hull is modeled using RANS equations employing the Finite volume method (FVM). Water is assumed incompressible in calculations, thus the volume of water entering computational cells in vicinity of ship's hull will match with an equal volume of water flowing out, leads to continuity equation. Together with Navier-Stokes equations, conservation of momentum of the flow can be defined and flow field around ship's hull can be characterized. Formulations and details of the numerical methodologies in CFD are well documented in many literatures. Thus, only the main features of the methodologies described.

2.1 Governing Equation

The governing equations applied in this study are instantaneous conservation of mass (continuity equations) and momentum (RANS) for incompressible turbulence flow. These equations are expressed in Cartesian tensor form as follows:

$$\frac{\partial \rho}{\partial t} + \frac{\partial}{\partial x_i}(\rho u_i) = 0 \quad (1)$$

$$\frac{\partial}{\partial t}(\rho u_i) + \frac{\partial}{\partial x_i}(\rho u_i u_j) = -\frac{\partial p}{\partial x_i} + \frac{\partial}{\partial x_j}\left[\mu\left(\frac{\partial u_i}{\partial x_j} + \frac{\partial u_j}{\partial x_i} - \frac{2}{3}\delta_{ij}\frac{\partial u_l}{\partial x_l}\right)\right] + \frac{\partial}{\partial x_i}\left(-\rho\overline{\acute{u}_i\acute{u}_j}\right) \quad (2)$$

Where u_i is the time averaged velocity components in Cartesian coordinates $x_i (i = 1, 2, 3)$, p, ρ and μ are the static pressure, fluid density and fluid viscosity respectively, δ_{ij} is the Kronecker delta and $-\rho\overline{\acute{u}_i\acute{u}_j}$ is the Reynolds stress, where

$$-\rho\overline{\acute{u}_i\acute{u}_j} = \mu_t\left(\frac{\partial u_i}{\partial x_j} + \frac{\partial u_j}{\partial x_i}\right) - \frac{2}{3}\left(\rho k + \mu_t\frac{\partial u_k}{\partial x_k}\right)\delta_{ij} \quad (3)$$

2.2 Turbulence Model

To close the RANS equations, a classical 2-equation eddy viscosity model, shear-stress transport (SST) k–ω model[15] was used, where

$$\frac{\partial}{\partial t}(\rho k) + \frac{\partial}{\partial x_i}(\rho k u_i) = \frac{\partial}{\partial x_j}\left(\Gamma_k\frac{\partial k}{\partial x_j}\right) + \tilde{G}_k - Y_k + S_k \quad (4)$$

$$\frac{\partial}{\partial t}(\rho\omega) + \frac{\partial}{\partial x_i}(\rho\omega u_i) = \frac{\partial}{\partial x_j}\left(\Gamma_\omega\frac{\partial \omega}{\partial x_j}\right) + G_\omega - Y_\omega + D_\omega + S_\omega \quad (5)$$

In these equations, $\tilde{G}_k$ and G_ω represents the generation of turbulence kinetic energy due to mean velocity gradients and generation of ω. The effective diffusivity for the SST k–ω model represented by $\Gamma_k$andΓ_ω. The term Y_k represents the dissipation of turbulence kinetic energy and term Y_ω represents dissipation of ω. Cross-diffusion term of the model is given by D_ω, and S_k and S_ω are user-defined source terms. The SST k–ω model remained as one of the most accurate and reliable turbulence models for external hydrodynamics[14].

■3.0 SIMULATION DESIGN AND ANALYSIS METHODS

3.1 Experiment

A series of model experiments were conducted in order to measure the resistance of the LNG model. All the experiments in this article are conducted in the 120 m long towing tank at Marine Technology Centre (MTC) of Universiti Teknologi Malaysia (UTM) in deep water conditions. The LNG model contains an open stern-form with buttock flow line and a wide central skeg. The principal dimensions of LNG tanker are presented in Table 1 and the model ship was manufactured with scaling ratio 112. The ship model is free to heave and pitch and towed in bare hull condition. A glimpse of the hull form has been portrayed in Figure 1.

Table 1 Principal dimensions of the ship and model

Principal particulars	Full scale	Model
Length between perpendicular (L) in meters	266	2.375
Beam (B) in meters	41.6	0.371
Draft (d) in meters	11.13	0.099
Block coefficient (C_b)	0.746	0.746

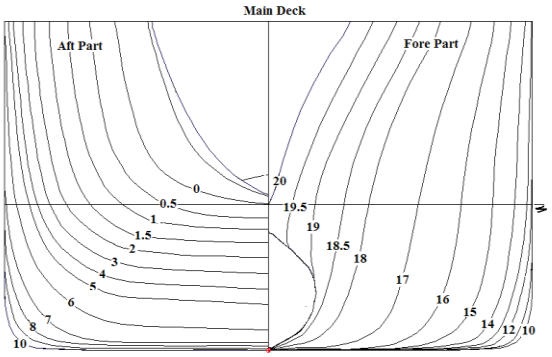

Figure 1 Body plan of the LNG carrier

3.2 Computational domain and boundary conditions

For present study, the hull form chosen is a typical LNG model with central skeg. The domain made up by seven boundaries: hull surface, flow pressure inlet, flow pressure outlet, top and bottom as well as two side walls. Schematic diagram indicating the computational domain is given in Figure 2. Location of the hull, tank bottom and two side walls are corresponding to the towing tank with smooth walls and no-slip condition imposed. Hydrostatic pressure at outlet boundary was calculated as function of water volume fraction. Calculations were performed in model scale with standard wall function used.

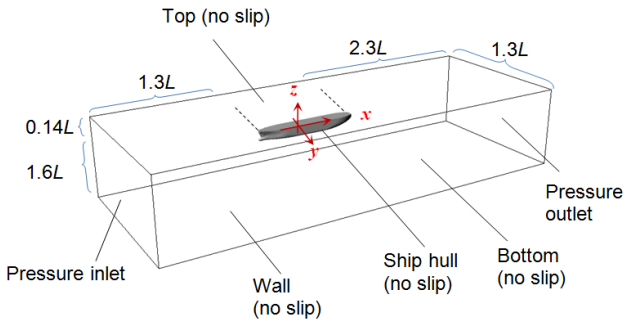

Figure 2 Boundary conditions of the computational domain

3.3 Grid generation

The computational domains are discretized with multi-block grid approach. Structured grids are exploited to attain high quality meshes and for the ease of boundary layers refinement purposes. A set of three geometrical similar grids with different grid spacing in three directions are generated by grid generator ICEM CFD. Clusters of grid points are concentrated in the hull and free surface regions as shown in Figure 3. The three systematically varied grids set were created with uniform grid refinement factor, $r = h_{i+1}/h_i = \sqrt[3]{2}$ where h_{i+1} and h_i are the grid spacing of two successively refined grids with h_i corresponding to the grid spacing of finest grid. Since the value of y^+ is flow dependent, the grids are designed with 20 cells within boundary layer with the first grid point away from ship hull refined to $y^+ = 50$ for every Froude number tested. The dimensions of the three grids are summarized in Table 2.

Table 2 Description of grids

No.	Grid points	h_i/h_1
Grid – 1 (fine)	4,103,026	1
Grid – 2 (medium)	1,810,370	1.260
Grid – 3 (coarse)	857,626	1.587

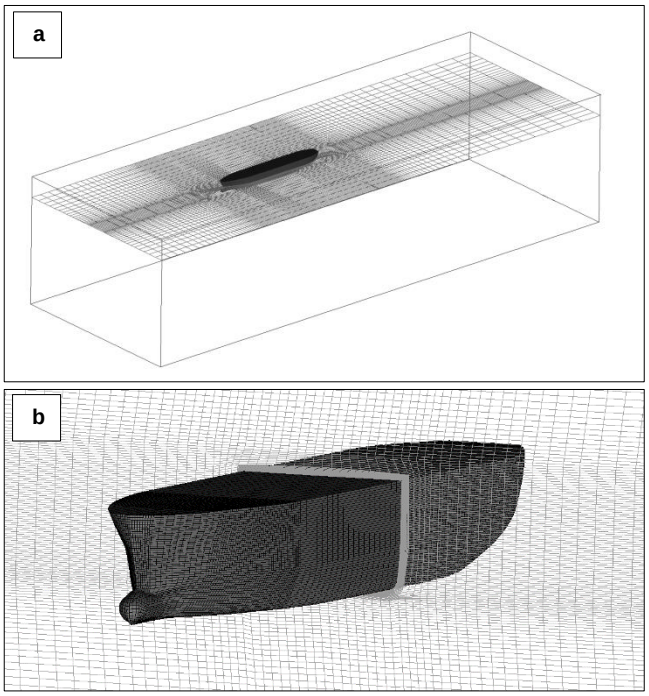

Figure 3 Computational grid topology: **a** Overview of the grid, **b** Frontal view of the ship with refinement on the surface grid around ship

3.4 Computational Setup and Numerical Simulation

The SIMPLE-Consistent[16] algorithm is used to couple the momentum and continuity equations. Pressure Staggering Option (PRESTO!) scheme is used for pressure interpolation while other terms are discretized using a second order upwind method. Volume fraction equations solved by High Resolution Interface Capturing (HRIC) scheme[17].

Convergence was assessed by ensures the drag converge to steady state and residuals scaled by the initial imbalance of equations drop four orders of magnitude. The simulation condition in this study is showed in Table 3. Viscous flow field around LNG model at eight different Froude number ranging from 0.1309 to 0.2072 corresponded to 13 knot to 20 knot in real ship are computed.

Simulations are run on a shared-memory type machine with 4 processors (3.6 GHz). The computing time for finest grid (Grid-1) used 4 processors required roughly 30 wall clock hours. It must be emphasize that the ship model is fixed at even keel for all simulations, whereas experiments are performed with ship model free in heave and pitch motion.

Table 3 Simulation conditions

Case	*Fn*	*Rn* (×10^6)	Full scale speed (knots)	Model scale speed (*m/s*)	Grid system
1	0.1309	1.738	12.6	0.63	1, 2, 3
2	0.1450	1.925	14	0.70	1, 2, 3
3	0.1554	2.062	15	0.75	1, 2, 3
4	0.1657	2.200	16	0.80	1, 2, 3
5	0.1761	2.337	17	0.85	1, 2, 3
6	0.1865	2.475	18	0.92	1, 2, 3
7	0.1968	2.612	19	0.95	1, 2, 3
8	0.2072	2.750	20	1.00	1, 2, 3

3.5 Resistance characteristics

The total resistance R_T is decompose of frictional resistance R_F and pressure resistance R_P. In experimental method, frictional resistance is defined by ITTC-57 ship model correlation line. Sum of wave and hydrostatic terms are defined as residual resistance R_R and assumed equivalence to pressure resistance, where pressure resistance $R_P = R_T - R_F$. In CFD method, the frictional resistance R_F and pressure resistance R_P are computed as integral of tangential stresses and normal stresses over the hull.

Total resistance coefficient C_T is expressed by non-dimensionalized R_T as

$$C_T = \frac{R_T}{\frac{1}{2} \times \rho \times S \times V^2} \quad (6)$$

where$S$ is the wetted hull surface area in still water. The frictional resistance coefficient, C_F, in accordance with the ITTC-57 formula is defined by:

$$C_F = \frac{0.075}{(\log Rn - 2)^2} = \frac{R_F}{\frac{1}{2} \times \rho \times S \times V^2} \quad (7)$$

The pressure resistance coefficient, C_P is calculated as $C_T - C_F$.

■4.0 RESULTS AND DISCUSSION

4.1 Grid Independent Study

In the grid independent study, the solution change between fine and medium grid ε_{21} is mostly below 1% of fine grid solution S_1, whereas the solution change between medium and coarse grid ε_{32} is close to 4% $S1$. ε_{21} is smaller at approximate 2.5 times ε_{32}. Figure 4 shows the comparison of total resistance from CFD prediction over different grid system and experiment measurement.

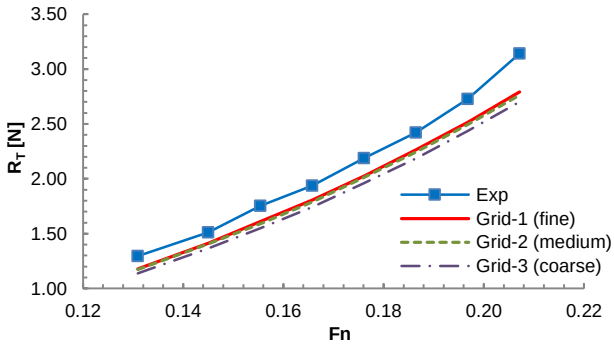

Figure 4 Comparison between experimental and computational R_T over different grid system

4.2 Resistance characteristics

Figure 5 shows the trend of total resistance coefficient C_T from CFD prediction for fine grid system and experiment measurement, also shown is decomposition of the resistance elements. The experiment data shows the largest C_T at the lowest speed Fn=0.1309, followed by a decrease as the speed is increased to Fn=0.1450. A further increase in speed produces an increase in the C_T curve at roughly Fn=0.1554, followed by a decrease up to Fn=0.1657. The C_T curve remain steady since then up to Fn=0.1968 except a slide decrease at Fn=0.1865. Further increase in speed record the second largest C_T in the curve at highest speed Fn=0.2072.

CFD data show a decrease from maximum C_T near lowest speed Fn=0.0309 up to the minimum at the highest speed Fn=0.2072. Compared to the experimental data, the computational results are under predicted from 6.4% to 11.2% of experimental value, which may attribute to the different running attitudes between CFD and experiment where model is fixed and even keel in CFD while physical model in towing tank experience free trim changes and squat.

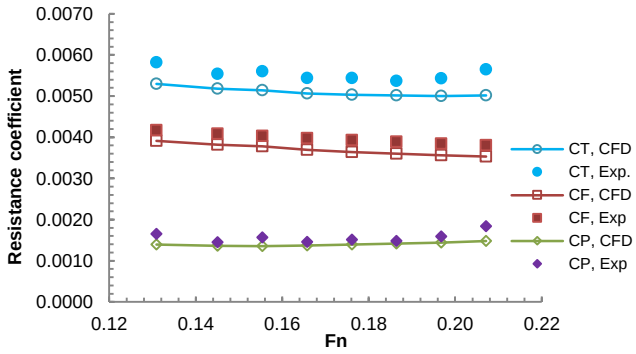

Figure 5 Comparison of resistance coefficients between computational and experimental results (grid-1)

The computed results are summarized in Table 4, showing the composition of frictional and pressure resistance components together with the validation comparison error of C_T. Overall trends are encouraging in that the computational results agree with the experimental data within the error of 11.2% and all the quantities follow the trends of the experimental data well over the entire range of speeds. High validation comparison error at the highest Froude number may indicates the difficulties in resistance

prediction due to high wave making resistance. More mesh elements around the hull are required, which could not be attained due to limitation in computational resources.

The computed ratios of frictional and pressure resistance coefficient are 69.1% and 30.9%, respectively, with respect to the total resistance coefficient at lowest speed *Fn*=0.1309, and become 66.6% and 33.4%, respectively, at the highest speed *Fn*=0.2072. The predictions are well consistence with experiment where frictional and pressure resistance coefficient are 71.1% and 28.3%, respectively, at the lowest speed and 67.4% and 32.6% at the highest speed, attributable to the increase of pressure components due to free surface deformation around the ship hull.

The CFD calculations show a maximum pressure resistance coefficient at *Fn*=2072 which is consistence with experiment. Remarkable accuracy of the computation is achieved particularly from *Fn*=0.1657 to *Fn*=0.1865, with difference of -6.2%, -7.9% and -4.5%. However the variations of pressure resistance coefficient with Froude number in experiment are not captured. The computed frictional resistance coefficient was under-predicted in general by average 6.9% compared to experiment. The overall variation of the frictional resistance coefficient with Froude number is successfully captured and well consistent with experiment.

Figure 6 shows the resistance ratio C_P/C_F from CFD calculations and experiment. The C_P/C_F is initially decrease and shows the minimum at *Fn*=0.1450 experimentally, followed by increase and show a local maximum at *Fn*=0.1554. Further increase in speed produces a decrease at *Fn*=0.1657 followed by increase with further speed increment from *Fn*=0.1761 and show maximum at the highest speed *Fn*=0.2072, with the exception of a slide decrease at *Fn*=0.1865.

It is found that frictional components dominate in the resistance of current model with the pressure components increases with higher speed. CFD data show a similar trend with an increase from the minimum C_P/C_F at lowest speed *Fn*=0.1309 up to the maximum at highest speed *Fn*=0.2072. Comparison between CFD and experiment is considered to be showed the ability of RANS code in predicting resistance coefficient over the tested range of Froude number.

Table 4 Computed resistance coefficient and validation comparison error

Fn	C_F (x 10^3)	C_P (x 10^3)	C_T (x 10^3)	*E*
0.1309	3.910	1.390	5.300	-8.95
0.1450	3.816	1.362	5.177	-6.44
0.1554	3.783	1.358	5.141	-8.16
0.1657	3.698	1.367	5.065	-6.81
0.1761	3.643	1.391	5.033	-7.46
0.1865	3.602	1.415	5.017	-6.52
0.1968	3.565	1.438	5.004	-7.85
0.2072	3.532	1.481	5.013	-11.17

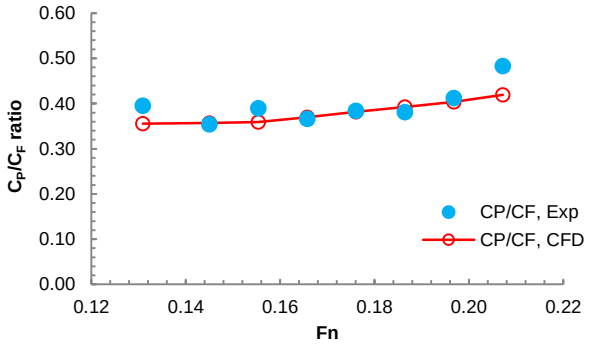

Figure 6 Comparison of resistance ratio C_P/C_F in CFD and experiment

4.3 Free Surface

The study of free surface wave profile around the hull is crucial to study the wave resistance. Figure 7 shows the computed free surface wave elevation at *Fn* = 0.1657, 0.1865 and 0.2072. Typical Kelvin wave pattern with symmetric and diverging waves dominated by bow and stern wave systems are observed.

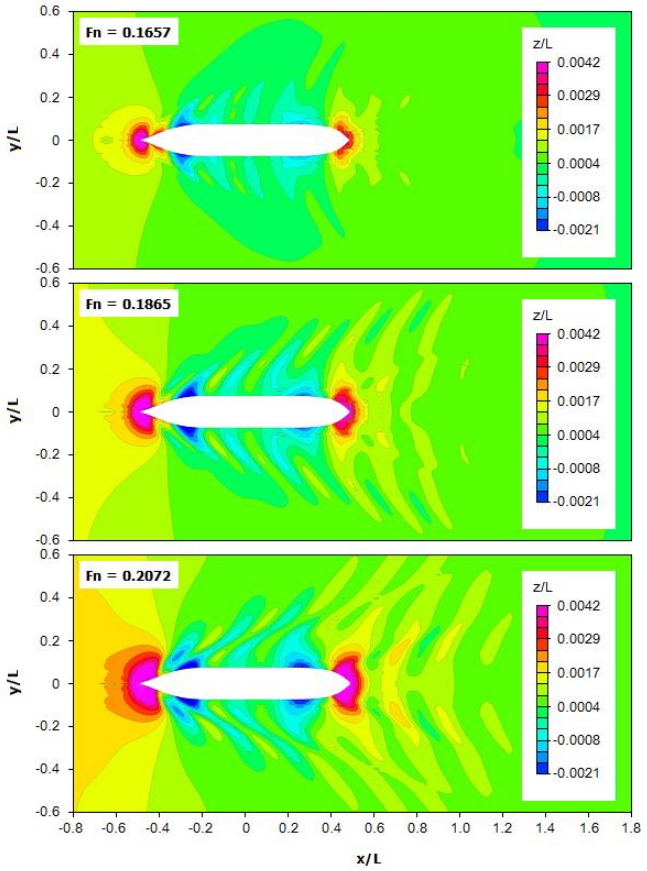

Figure 7 Free surface elevation at *Fn* = 0.1657, 0.1865 and 0.2072 (grid-1)

The diverging wavelength agree very well with calculated wavelength based on linear wave theory, $\lambda = 2\pi \times Fn^2 \approx 0.17$, 0.22 and 0.27 as the Froude number increased from 0.1657, 0.1865 and 0.2072. Compared to the cases at lower Froude numbers, the diverging waves at higher Froude numbers shed

further away from the hull. Bow wave in simulations are successfully resolved and illustrated in Figure 8.

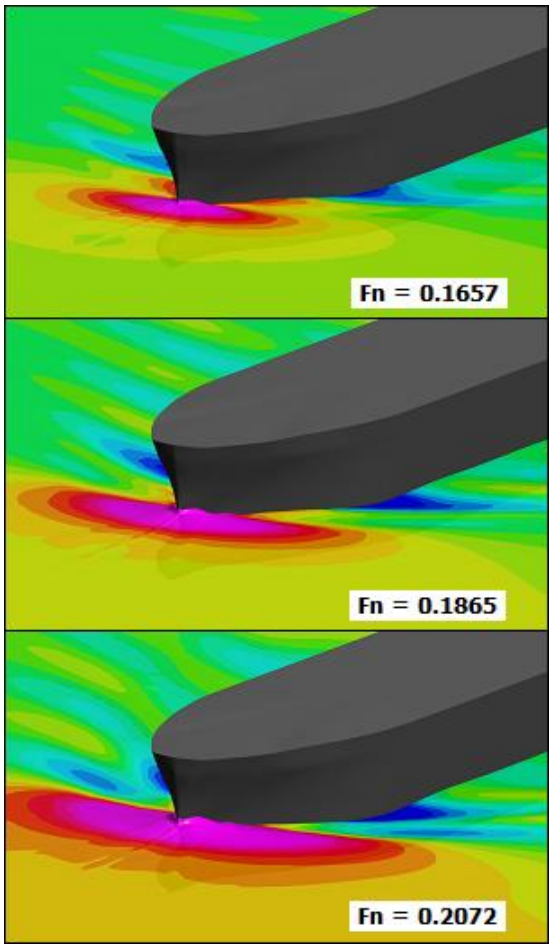

Figure 8 Predicted free surface with bow wave for *Fn* = 0.1657, 0.1865 and 0.2072

Figure 9 presents the wave profile along the LNG hull form at different Froude numbers. Overall wave profiles between different Froude numbers are similar with local differences. The wave profiles are more developed for cases in higher Froude number. Wavelength is varying with three wave crest observed at the midship region for the cases of *Fn* = 0.1450 and 0.1657 while two wave crest observed for the cases of *Fn* = 0.1865 and 0.2072.

Significant magnitude difference observed at the trough of ship bow and stern. Amplitude at highest *Fn* = 0.2072 are more pronounce compared to *Fn* = 0.1450, up to 71% at bow and 94% at stern, which is effectively doubled. This explained the increase of C_P/C_F ratio with increase of speed that caused by the pressure change due to differential change in wave profile. Wave crest and trough at midship regions are almost the same in amplitude for all Froude numbers studied.

It must be commented that wave pattern is mainly governed by pressure field and mass forces. Thus, the comparison of such patterns obtained in the course of experiment and simulations contributes the verification of results. It would be informative to collate the graphic based on CFD simulations with photo taken in future during experiment if it is feasible.

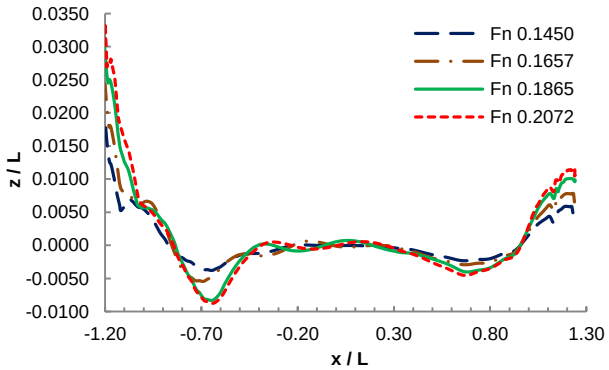

Figure 9 Wave profile along the hull at different Froude number (grid-1)

5.0 CONCLUSION

RANS simulations are performed for LNG hull form using general purpose RANS solver Fluent. Resistance characteristics and viscous free surface of the model are examined at a wide range of Froude numbers. Prediction of resistance by CFD are satisfactory, evidenced by differences less than 11.2% compared to the experiment and the overall resistance tendencies followed well to the experimental data for entire range of speeds. The prediction also shown ratio of C_P/C_F in resistance consistent with experiment.

Overall, ability of current solver in predicting accurate value of resistance coefficient is confirmed, reveal the feasibility of RANS method in practical marine hydrodynamics application. Differences between the CFD and experimental data are expected due to inconsistency in running attitudes between CFD and experiment. Studies are required to investigate the effect of more advanced turbulence models, finer grid and covering trim and sinkage in CFD for more practical prediction of resistance characteristics in future.

Acknowledgement

The presented work is support by Marine Technology Center (MTC) and Centre for Information and Communication Technology (CICT) in Universiti Teknologi Malaysia. The authors would like to express their sincere gratitude to Ministry of Science, Technology and Innovation (MOSTI) Malaysia for financial support given to the research.

References

[1] Larsson, L., Baba, E. 1996. *Ship Resistance and Flow Computations.Advances in Marine Hydrodynamics*. Ohkusu, M. (editor), Southampton: WIT Press. 1–75.
[2] Larsson, L. 1997. CFD in ship design–Prospects and Limitations. *Ship Technology Research*. 44: 133–154.
[3] Bertram, V. 1998. Marching Towards the Numerical Ship Model Basin.*Proceedingsof Euromech Conference 374*. Poitiers, France. 3–17.
[4] Larsson, L., Stern, F., Visonneau, M. 2013. *Numerical Ship Hydrodynamics: An Assessment of the Gothenburg 2010 Workshop*. Heidelberg: Springer.
[5] ITTC. 2011. The Specialist Committee on Uncertainty Analysis. *Proceedings of 26th ITTC*. Rio de Janeiro, Brazil. 1: 299–335.
[6] Hakan Ozdemir, Y., Bayraktar, S., and Yilmaz, T. 2007. Computational Investigation of a Hull. *Proceedingsof 2nd International Conference on Marine Research and Transportation (ICMRT 07)*. Naples, Italy.
[7] Eca, L., Hoekstra, M. 2009. On the Numerical Accuracy of the Prediction of Resistance Coefficient in Ship Stern Flow Calculations. *Journal of Marine Science and Technology*. 14: 2–18.

[8] Hino, T., Ohashi, K., and Kobayashi, H. 2010. Flow Simulations Using Navier-Stokes Solver Surf. *Proceedings of Gothenburg 2010 Workshop on Numerical Ship Hydrodynamics*. Gothenburg, Sweden.
[9] Kim, J., Park, I. R., Kim, K. S., and Van, S. H. 2010. Feasibility Study on Numerical Towing Tank Application to Predictions of Resistance and Self-Propulsion Performances for a Ship. *Proceedings of Gothenburg 2010 Workshop on Numerical Ship Hydrodynamics*. Gothenburg, Sweden.
[10] Wilson, R. V., Carrica, P. M., and Stern, F. 2006. URANS Simulations for a High-Speed Transom Stern Ship with Breaking Waves.*International Journal of Computational Fluid Dynamics*. 20(2): 105–125.
[11] Stern, F., Huang, J., Carrica, P., Yang, J., Ghosh, S., and Van, S. 2006. Two-Phase CFD and PIV EFD for Plunging Breaking Waves, Including Alternative CFD Approaches and Extensions for Air/Water Ship Flow.*Proceedings of 26th Symposium on Naval Hydrodynamics*. Rome, Italy.
[12] Maki, K. J., Broglia, R., Doctors, L. J., and Mascio, A. D. 2013. Numerical Investigation of the Components of Calm-Water Resistance of a Surface-Effect Ship.*Ocean Engineering*. 73: 375–385.
[13] Zwart, P. J., Godin, P. G., Penrose, J., and Shin, H. R. 2008. Simulation of Unsteady Free-Surface Flow around a Ship Hull Using a Fully Coupled Multi-Phase Flow Method. *Journal of Marine Science and Technology*. 13: 346–355.
[14] Fonfach, J. M. A., GuedesSoares, C. 2010. Improving the Resistance of a Series 60 Vessel with a CFD Code. *Proceedings of V European Conference on Computational Fluid Dynamics*. Lisbon, Portugal.
[15] Menter, F. R. 1994. Two-Equation Eddy-Viscosity Turbulence Models for Engineering Applications. *AIAAJournal*. 32(8): 1598–1605.
[16] Van Doormaal, J. P. and Raithby, G. D. 1984.Enhancements of the SIMPLE Method for Predicting Incompressible Fluid Flows. *Numerical Heat Transfer*. 7: 147–163.
[17] Muzaferija, S. Peric, M., Sames, P., and Schellin. T. 1998. A Two-Fluid Navier-Stokes Solver to Simulate Water Entry. *Proceedings of 22nd Symposium on Naval Hydrodynamics*. Washington, DC. 277–289.